Solar Energetic Particle events observed by Solar Orbiter

Author: Arnau Serra Garet
Facultat de Física, Universitat de Barcelona, Diagonal 645, 08028 Barcelona, Spain.

Advisor: Maria dels Àngels Aran Sensat

Abstract: Solar energetic particle events are a component of the space weather. Understanding their generation and evolution is essential to mitigate their hazardous effects. By using data collected by the Solar Orbiter spacecraft, this work analyses and interprets the electron directional intensities for two events. With the help of interplanetary magnetic field observations, we determine the electron pitch-angle distributions at different times during the events, and conclude that the transport of the electrons was dominated by focusing in one case and modulated by scattering off magnetic field fluctuations in the other instance.

I. INTRODUCTION

During a solar energetic particle (SEP) event, charged particles from the sun are accelerated by solar activity. SEPs can be accelerated mainly by solar flares and coronal mass ejections (CME), which generally are classified broadly as impulsive or gradual events [1]. These particles travel through the solar wind plasma at nearly relativistic speeds and become a potential danger to the electronic components on satellites. Thus, the study of space weather and specially of SEP events is of great interest to avoid these potential hazards.

Different missions have been launched to study the Heliosphere and space weather during the last five decades. Recently, Solar Orbiter (SolO), launched on the 10^{th} of February 2020, joined the fleet of existing platforms to deepen into the understanding of the sun, its activity and the interplanetary space [2]. Since then, SolO has been orbiting around the Sun collecting in-situ measurements, i.e. solar energetic particle intensities, solar wind plasma parameters and interplanetary magnetic field (IMF), and more sporadically from remote-sensing measurements, e.g. x-ray emissions, radio emissions, magnetograms and euv images.

This work presents a study of two SEP events measured by SolO in 2020. The first event occurred on the 22^{nd} of October when SolO was located at 0.99 au from the Sun, and the second on the 10^{th} of December when SolO was at 0.82 au. Fig.1 shows the positions of SolO (black curve), Earth (light blue) and other planets. In both events, SolO is situated at almost the opposite position of the Earth with respect to the Sun.

By making use of different physical magnitudes such as the IMF and electron intensities, we aim at understanding some of the physical processes behind solar energetic particles events. Firstly a brief description of the particle transport processes involved is presented in section II. Secondly, a description on the data collected and its treatment is given in section III. Next, results are presented and analysed in section IV, and finally, conclusions are drawn in section V.

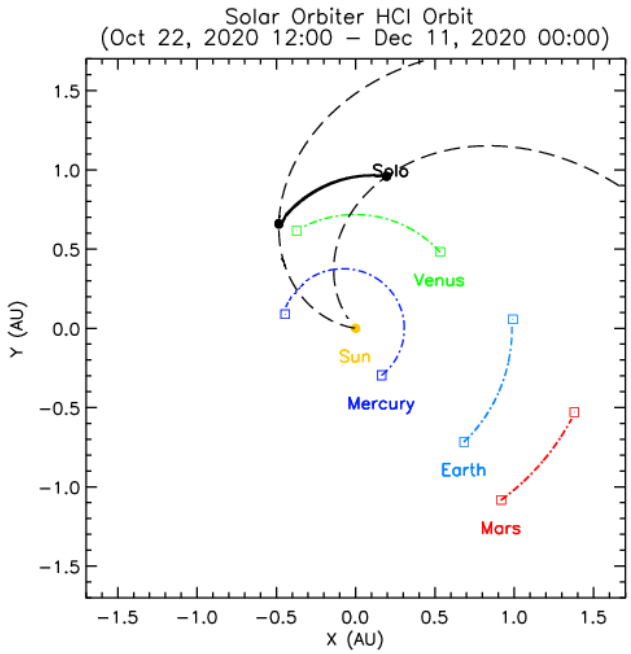

FIG. 1: Representation showing the trajectory in heliocentric inertial coordinates of Solar Orbiter (marked as 'solo') and nearest planets between the first event (22^{nd} of October), and the second event (10^{th} of December). The Parker spirals through Solar Orbiter are also shown. Edited from [3].

II. PHYSICAL PROCESSES

Solar wind is a moving plasma generated from the expanding outer layer of the Sun. Due to its high conductivity, the frozen in condition can be applied and the IMF travels embedded in the solar wind plasma. Although the solar wind expands nearly radially, the Sun's rotation, with a mean period of 27.3 days, curves the IMF lines into an Archimedean spiral shape known as Parker spiral [1]. Then the path length of the particles along the Parker spiral corresponds to:

$$z(r) = \frac{a}{2}\left[\frac{r}{a}\sqrt{1+\frac{r^2}{a^2}} + \ln\left(\frac{r}{a}+\sqrt{1+\frac{r^2}{a^2}}\right)\right] \qquad (1)$$

Where r is the radial distance from the Sun and $a = \frac{u}{\Omega}$ with u the solar wind speed and Ω the solar angular rotation speed.

Once SEPs have been accelerated by solar flares or CMEs and escape into the interplanetary space, they travel with an helicoidal movement along the IMF lines. The particles' velocity can be divided into two components, $v_{\parallel}$ parallel and $v_{\perp}$ perpendicular to the magnetic field. In a collisionless plasma like the solar wind, and neglecting any other external force, the motion of a charged particle in a magnetic field is described by,

$$m\frac{d\vec{v}}{dt} = q\left(\vec{v}\times\vec{B}\right). \tag{2}$$

From Eq.(2), and assuming a constant magnetic field, it can be deduced that the particle travels at a constant speed, $v_{\parallel}$, in the direction parallel to $\vec{B}$ while it describes a gyration motion in the perpendicular plane, with a *Larmor radius* of $r_L = \frac{mv_{\perp}}{|q|B}$. An extended derivation can be found on [4, Chapter 2].

Defining the pitch angle as,

$$\alpha = \tan^{-1}(v_{\perp}/v_{\parallel}), \tag{3}$$

it can be seen that for a moving particle with $v_{\parallel} = 0$, its trajectory would be circular around the magnetic field with a pitch angle of 90°. On the other hand for a $v_{\perp} = 0$ the particle would move along the magnetic field with a pitch angle of 0°.

However, the IMF is not constant, its intensity decreases with increasing radial distance from the Sun. In a slow changing magnetic field, the magnetic moment remains constant (it is the first adiabatic invariant). Thus, the transverse kinetic energy of a charged particle moving further from the Sun decreases while the parallel kinetic energy increases [4, Chapter 3]. Then, the pitch angle of the particle, Eq.(3), would decrease approximating to zero. This process is called focusing. Additionally, particles get scattered in pitch angle due to IMF fluctuations. Therefore, the pitch-angle distribution of SEP events is a result of two competing transport processes: focusing and scattering [1].

III. OBSERVATIONS AND METHODOLOGY

Solar Orbiter is equipped with the Energetic Particle Detector (EPD, [5]), that consist of four sensors, designed to measure the composition, energy spectra and directional intensities of energetic particles for a wide range of energies.

For the purpose of this work, we use electron differential intensities from the Electron Proton Telescope (EPT) sensor. EPT has two units, one pointing sunward and anti-sunward along the Parker spiral (obtained from measurements from the Helios spacraft, 35° westward from the Sun-SolO line [5]) and another one pointing southward and northward, with a 35° tilt from the North ecliptic pole, and 90° westward from the Parker spiral direction. Therefore, EPT provides four 30°-fields of view (FOV) (sun, asun, north and south).

The electron directional intensities are provided with a cadence of 1 second and distributed in 17 energy channels covering an energy range from 31.86 keV to 471.00 keV. The pitch angle of the electrons entering through each FOV is calculated as,

$$\mu = \cos\alpha = \hat{s}\cdot\frac{\vec{B}}{B} \tag{4}$$

where $\hat{s}$ is the flow unit-direction of the particles entering through the centre of each FOV. The flow direction is provided by the EPT instrument team in Radial-Tangential-Normal (RTN) spacecraft centred coordinates with a 1-minute cadence. For the IMF, measurements of the field components in the same reference frame and cadence from the magnetometer (MAG, [6]) were used. All data used in this work were retrieved from the Solar Orbiter Archive [7].

For the analysis of the pitch-angle distributions (PADs), we calculated 1-minute averages of the particle intensities for the December event whereas 5-minute averages were used for the October event to reduce noise. Next, normalised intensities as a function of μ are obtained for six times throughout the events: at the half height of the peak, at the peak and four times along the decay. PADs allows us to further understand the event directional intensities.

The time of flight, from the Sun to SolO along the IMF, Eq.(1), for the electrons with $\mu = 0$ and for each energy channel, were computed to estimate if the temporal averages used were a significant portion of the travelling time of the electrons. For this, we determined a solar wind speed of 400 km s^{-1} from measurements of the Solar Wind Analyser (SWA, [8]) for the October event. We used the same speed for the December event as no solar wind data was available. Next, we determined the pre-event intensity level (termed as 'the background') as the mean value of the intensities from each FOV over 15 minutes, and identified the onset time of the particle intensities as the third value with higher intensity than two times the background's standard deviation.

To verify the Python code developed for this data analysis, the electron intensity and pitch angles obtained for another event occurred on the 22^{nd} of July were plotted and compared with published results [9].

IV. EVENT ANALYSIS

Figure 2 shows the electron intensity-time profiles for the 10^{th} of December (event number 1, left) and for the 22^{nd} of October (event number 2, right) for selected energy channels. The results of the analysis described in Section III is presented for the lowest energy channel. For the other energy channels the results obtained were

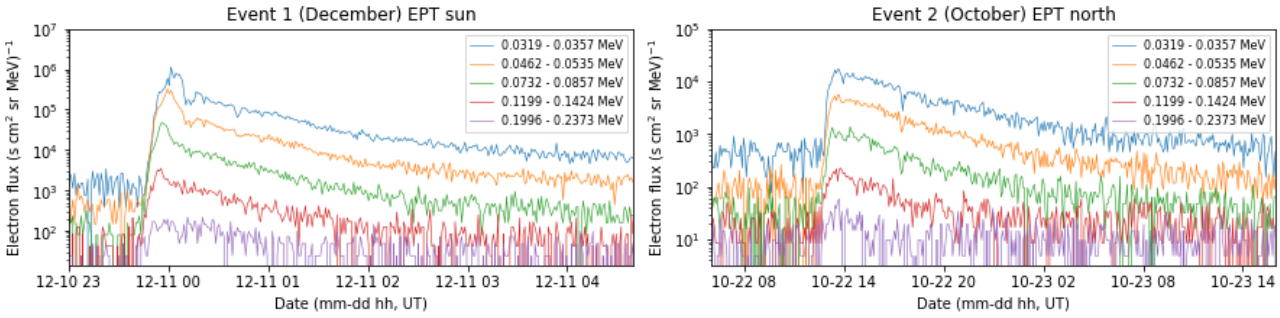

FIG. 2: Electron intensity-time profiles for five differential energy channels of the EPT sensor. Left: Measurements of the EPT Sun telescope for the December event. Right: Measurements of the EPT North telescope for the October event.

similar, yet the intensity decreased with increasing energy, preventing the analysis at the higher energies where intensities were only slightly above the background level.

For each event the computed onset, peak, background intensity and maximum intensity are presented in Table I. The ratio between the temporal average used and the electron time of flight was of 5 % for event 1 and 4 % for event 2.

Event number	1	2
Date (UT)	Dec 10-11	Oct 22
Onset (UT)	23:49 ± 1 min	12:57 ± 5 min
Peak time (UT)	00:01 ± 1 min	13:42 ± 5 min
Background Intensity (s cm^2 sr MeV)$^{-1}$	1942 ± 942	444 ± 191
Peak intensity (s cm^2 sr MeV)$^{-1}$	$(11 \pm 4) \cdot 10^5$	$(2 \pm 2) \cdot 10^4$

TABLE I: From top to bottom: the date, onset time, peak time, background intensity and maximum intensity for the two events.

A. Event number 1

For event number 1, the electron intensity measured by the EPT sun telescope (blue curve in the top panel of Fig.(3)) started rising at 23:49 UT on 10^{th} December and reached its maximum intensity (peak value) 12 minutes later (Table I). Next, the decay phase started until the intensity recovered the background. The other FOV started rising gradually after the peak at the sun telescope. On $\sim$ 02:00 UT on 11^{th} December intensities reached similar values for all FOVs and kept decaying approaching the background level. Each telescope scanned similar pitch angles throughout the entire event (second panel of Fig.(3)), this is because the magnetic field direction remained relatively constant throughout the event (two lower panels of Fig.(3)). Note that the IMF has a negative polarity, that is, it points towards the Sun.

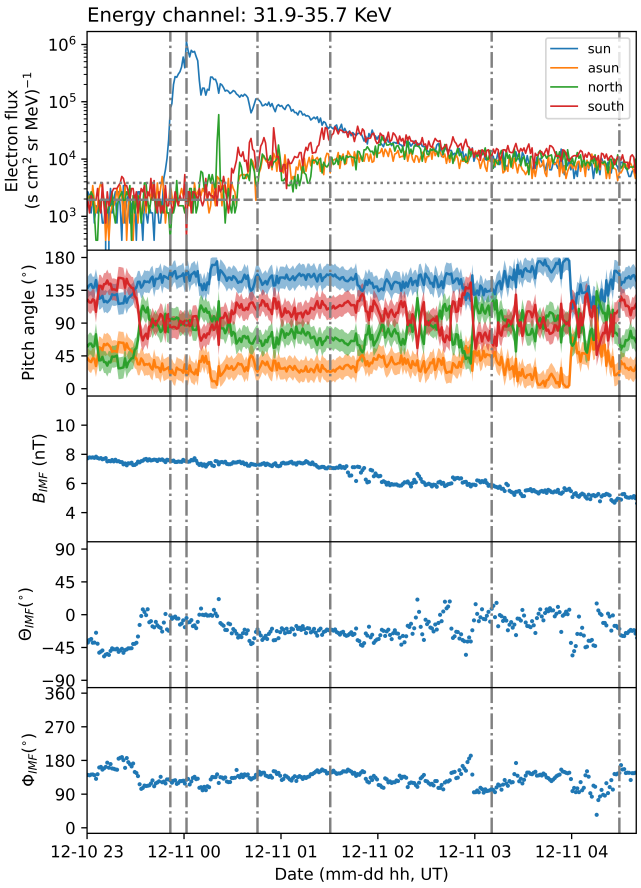

FIG. 3: Event number 1 (10^{th} of December). From top to bottom: 1) 31.9 – 35.7 keV electron intensities for each FOV (colour coded) with the background intensity (dashed line) and its two-times standard deviation (dotted line); 2) mean value of the pitch-angle (solid line) and coverage (shades) for each FOV (same colour code); 3) IMF intensity; 4) IMF latitude angle; 5) IMF azimuth angle. The vertical lines correspond to the times at which the PADs are studied.

The analysed PADs are shown in Fig.(4). The maximum intensity at the half-peak and peak times correspond to the Sun telescope, with $\mu \sim -0.92$, while the

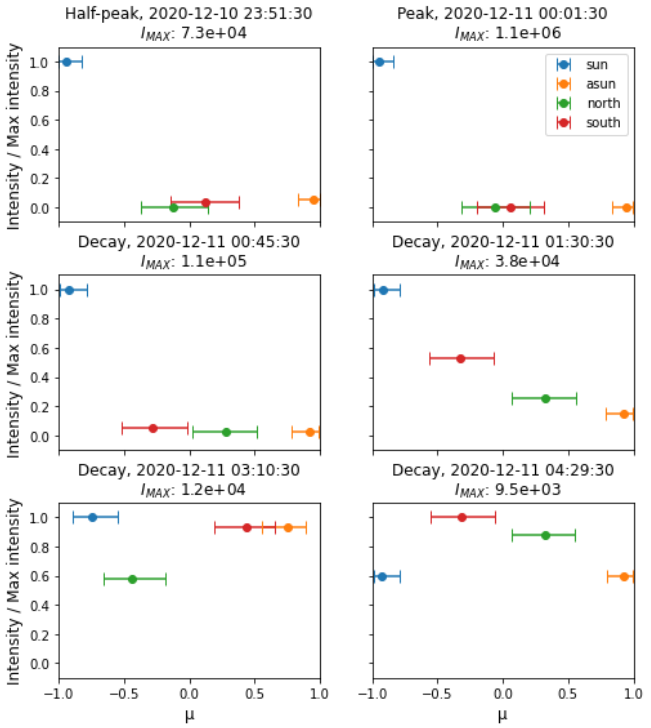

FIG. 4: Event number 1 (10^{th} of December). PADs for six times: Half-peak, Peak and four times during the decay, as indicated in each panel. Intensities have units of (s cm^2 sr MeV)$^{-1}$ and maximum values are indicated.

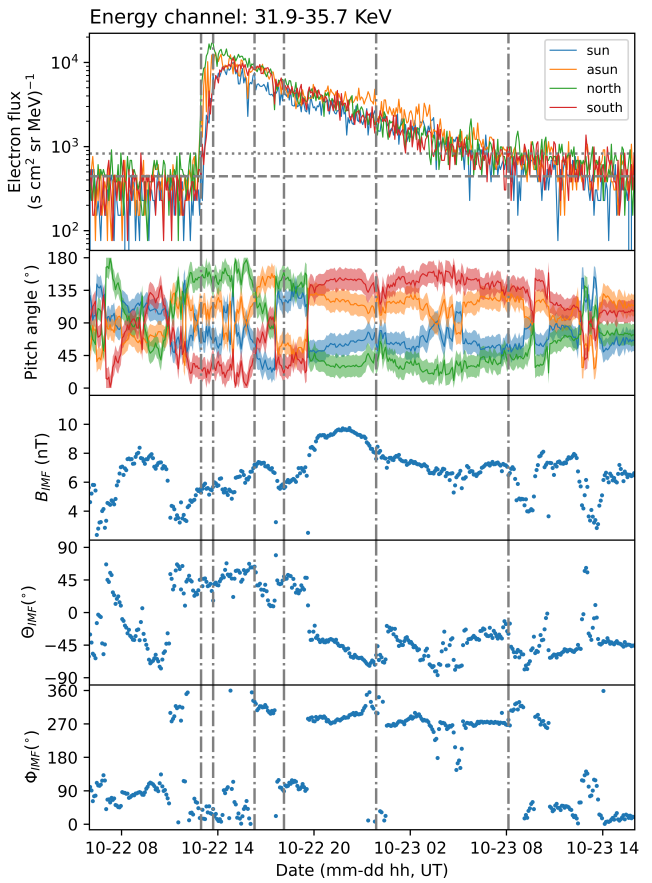

FIG. 5: Event number 2 (22^{nd} of December). From top to bottom: 1) 31.9 − 35.7 keV electron intensities for each FOV (colour coded) with the background intensity (dashed line) and its two-times standard deviation (dotted line); 2) mean value of the pitch-angle (solid line) and coverage (shades) for each FOV (same colour code); 3) IMF intensity; 4) IMF latitude angle; 5) IMF azimuth angle. The vertical lines correspond to the times at which the PADs are studied.

other FOV remained at the background level. At this times, the PADs are strongly anisotropic. During the decay, the PADs gradually isotropized after 01:30 UT on 11^{th} December while intensity values in all FOV decreased. PADs show that at the beginning of the event, particles flew mostly in the sunward direction $\mu \sim -1$, closely aligned with the IMF. The anisotropy is remarkably large, suggesting that particle transport was dominated by magnetic focusing.

The PADs obtained were compared with synthetic (modelled) and observed PADs from Helios spacecraft from other events [10, Chapter 5]. As expected, PADs corresponded to a beamed (focused) electron injection from the Sun and the other FOV electron intensities only increase later in the event due to the electrons scattered in the interplanetary medium. Thus, we conclude electrons were accelerated during a solar impulsive event, and travelled through an IMF line connected to Solar Orbiter, being focused by the diverging IMF.

B. Event number 2

For all FOV, the electron intensities rose closely in time and more gradually than for event 1 (top panel of Fig.(6). The north and asun FOVs show a prompter increase than the two other FOVs. After their respective peak values, the intensities show similar values for all FOV, with a slow decay to the background level. Pitch-angle changes reflect the variation of the IMF. Between the onset and the fourth time indicated in Fig.(6), the IMF intensity and latitude remain roughly constant and the azimuth angle showed two consecutive changes of sector, with changes in the IMF polarity from positive, negative to positive as calculated from MAG and SWA data, following Eq.(4.1) in [10]. A rotation and increase of the IMF followed this second change of sector.

Similarly to event 1, the PADs shown in Fig.(6) evolve from an anisotropic to an isotropic distribution, covering the full μ-domain. In contrast to event 1, the initial anisotropy is smaller and all FOVs reached similar intensity values well above the background level, indicating a higher level of scattering in the interplanetary space than for event 1.

Surprisingly the first to detect the event were the north and antisun FOVs, meaning that the electrons arrived

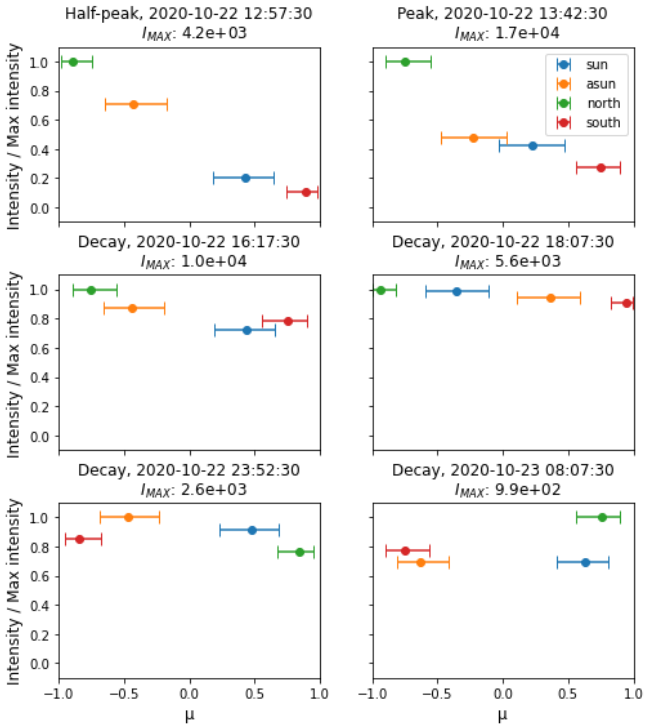

FIG. 6: Event number 2 (22^{nd} of December). PADs for six times: Half-peak, Peak and four times during the decay, as indicated in each panel. Intensities have units of (s cm^2 sr MeV)$^{-1}$ and maximum values are indicated.

at SolO from above and behind. The solar wind speed density and temperature time profiles (not shown here) suggest, together with the IMF data, that a small magnetic structure different from a shock or a CME swept by SolO. Given the opposite location of the Earth from SolO, we could not identify the solar source of such structure. SolO images from the Sun are not publicly available yet. Remote-sensing observations are needed to fully interpret this event.

V. CONCLUSIONS

We have analysed two solar energetic electron events by using in-situ measurements from the Solar Orbiter mission.

- The analysis of the electron directional intensities combined with IMF measurements enabled the interpretation of some of the physical processes involved in the particle transport in the interplanetary space. The PADs of the 10^{th} December event allow us to conclude that the transport of the electrons was governed by magnetic focusing, while the PADs of the 22^{nd} October event suggest a transport in a more turbulent interplanetary space, where pitch-angle scattering is stronger than for event 1.
- The Heliosphere is a complex scenario where SEP events propagate. In-situ measurements were sufficient to reach the goals initially presented, nevertheless, to fully understand event 2, remote-sensing observations are needed.

Acknowledgments

Solar Orbiter is a mission of international cooperation between ESA and NASA, operated by ESA. We thank the SolO/EPD i MAG teams for the public particle and magnetic field data products available. Also I would like to thanks my advisor Maria dels Àngels Aran Sensat for her guidance and support during all the project. Finally, to my colleagues with special consideration to Eloi Codina Torras for his support with some aspects of the Python coding.

[1] A. Aran, et al., *Charged Particle Transport in the Interplanetary Medium*, in Astrophysics and Space Science Library, Springer International Publishing, 2017, pp. 63–78. doi: 10.1007/978-3-319-60051-2_4.

[2] D. Müller, et al., *The Solar Orbiter mission*, A&A, vol. 642, p. A1, Sep. 2020, doi: 10.1051/0004-6361/202038467.

[3] *SRG Solar Orbiter Science Server*, Universidad de Alcalá. Accessed on: 9-June-2021. [Online]. Available: http://espada.uah.es/tools/soloorbit.

[4] Bittencourt, J.A., *Fundamentals of Plasma Physics*, 3rd edn. Springer, New York (2004).

[5] J. Rodríguez-Pacheco et al., *The Energetic Particle Detector*, A&A, vol. 642, p. A7, Sep. 2020, doi: 10.1051/0004-6361/201935287.

[6] T. S. Horbury et al., *The Solar Orbiter magnetometer*, A&A, vol. 642, p. A9, Sep. 2020, doi: 10.1051/0004-6361/201937257.

[7] *Solar Orbiter Archive*, ESA. Accessed on: 10-May-2021. [Online]. Available: http://soar.esac.esa.int/soar.

[8] Owen, C. et al., *The Solar Orbiter Solar Wind Analyser (SWA) suite*, A&A, vol. 642, A16, Oct. 2020, doi: 10.1051/0004-6361/201937259.

[9] R. Gomez-Herrero et al., *First near-relativistic solar electron events observed by EPD onboard Solar Orbiter*, A&A, Jan. 2021, doi: 10.1051/0004-6361/202039883.

[10] D. Pacheco, *Analysis and modelling of the solar energetic particle radiation environment in the inner heliosphere in preparation for Solar Orbiter*, Universitat de Barcelona, Aug. 2019, http://hdl.handle.net/2445/134743.